Neurobiology of Disease 163 (2022) 105603

Contents lists available at ScienceDirect

Neurobiology of Disease

journal homepage: www.elsevier.com/locate/ynbdi

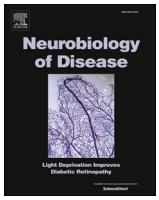

# S327 phosphorylation of the presynaptic protein SEPTIN5 increases in the early stages of neurofibrillary pathology and alters the functionality of SEPTIN5

Catarina B. Ferreira [a,b,1], Mikael Marttinen [c,d,1], Joana E. Coelho [a,b,1], Kaisa M.A. Paldanius [c], Mari Takalo [c], Petra Mäkinen [c], Luukas Leppänen [c], Catarina Miranda-Lourenço [a,b], João Fonseca-Gomes [a,b], Sara R. Tanqueiro [a,b], Sandra H. Vaz [a,b], Rita F. Belo [a,b], Ana Maria Sebastião [a,b], Ville Leinonen [e,f], Hilkka Soininen [g], Ian Pike [h], Annakaisa Haapasalo [j], Luísa V. Lopes [a,b], Alexandre de Mendonça [i], Maria José Diógenes [a,b,**], Mikko Hiltunen [c,*]

[a] *Instituto de Farmacologia e Neurociências, Faculdade de Medicina, Universidade de Lisboa, Lisboa, Portugal*
[b] *Instituto de Medicina Molecular João Lobo Antunes, Faculdade de Medicina, Universidade de Lisboa, Lisboa, Portugal*
[c] *Institute of Biomedicine, University of Eastern Finland, Kuopio, Finland*
[d] *Structural and Computational Biology, European Molecular Biology Laboratory, Heidelberg, Germany*
[e] *Institute of Clinical Medicine - Neurosurgery, University of Eastern Finland, Kuopio, Finland*
[f] *Department of Neurosurgery, Kuopio University Hospital, Kuopio, Finland*
[g] *Institute of Clinical Medicine - Neurology, University of Eastern Finland, Kuopio, Finland*
[h] *Proteome Sciences plc, London, United Kingdom*
[i] *Faculdade de Medicina, Universidade de Lisboa, Lisboa, Portugal*
[j] *A.I. Virtanen Institute for Molecular Sciences, University of Eastern Finland, Kuopio, Finland*

ARTICLE INFO

*Keywords:*
Aβ
Alzheimer's disease
APP processing
Autophagy
Post-translational modifications
SEPTIN5
Synaptic plasticity

ABSTRACT

Alzheimer's disease (AD) is the most common form of dementia, which is neuropathologically characterized by extracellular senile plaques containing amyloid-β and intracellular neurofibrillary tangles composed of hyperphosphorylated tau protein. Previous studies have suggested a role for septin (SEPTIN) protein family members in AD-associated cellular processes. Here, we elucidated the potential role of presynaptic SEPTIN5 protein and its post-translational modifications in the molecular pathogenesis of AD. RNA and protein levels of SEPTIN5 showed a significant decrease in human temporal cortex in relation to the increasing degree of AD-related neurofibrillary pathology. Conversely, an increase in the phosphorylation of the functionally relevant SEPTIN5 phosphorylation site S327 was observed already in the early phases of AD-related neurofibrillary pathology, but not in the cerebrospinal fluid of individuals fulfilling the criteria for mild cognitive impairment due to AD. According to the mechanistic assessments, a link between SEPTIN5 S327 phosphorylation status and the effects of SEPTIN5 on amyloid precursor protein processing and markers of autophagy was discovered in mouse primary cortical neurons transduced with lentiviral constructs encoding wild type SEPTIN5 or SEPTIN5 phosphomutants (S327A and S327D). C57BL/6 J mice intrahippocampally injected with lentiviral wild type SEPTIN5 or phosphomutant constructs did not show changes in cognitive performance after five to six weeks from the start of injections. However, SEPTIN5 S327 phosphorylation status was linked to changes in short-term synaptic plasticity *ex vivo* at

*Abbreviations:* AD, Alzheimer's disease; APP CTF, APP C-terminal fragment; APP, Amyloid precursor protein; APPim, Immature APP; APPm, Mature APP; Aβ, Amyloid-β; BACE1, β-site APP cleaving enzyme 1; CDK5, Cyclin-dependent kinase 5; CSF, Cerebrospinal fluid; fEPSPs, Field excitatory postsynaptic potentials; I/O, Input-output; IFNγ, Interferon γ; LPS, Lipopolysaccharide; LTP, Long-term potentiation; MCI, Mild cognitive impairment; PPF, Paired-pulse facilitation; PTM, post-translational modifications; S327A, Serine to alanine; S327D, Serine to aspartate; sAPPα/β, soluble APPα/β; SEPT, Septin; SNARE, Soluble N-ethylmaleimide sensitive fusion protein receptor; TNF-α, Tumor necrosis factor alpha.

* Correspondence to: M. Hiltunen, Institute of Biomedicine, University of Eastern Finland, Kuopio, Finland
** Correspondence to: M. J. Diógenes, Instituto de Farmacologia e Neurociências, Faculdade de Medicina, Universidade de Lisboa, Lisboa, Portugal.
*E-mail addresses:* diogenes@medicina.ulisboa.pt (M.J. Diógenes), mikko.hiltunen@uef.fi (M. Hiltunen).
[1] These authors contributed equally.

https://doi.org/10.1016/j.nbd.2021.105603
Received 10 September 2021; Received in revised form 2 December 2021; Accepted 22 December 2021
Available online 24 December 2021

the CA3-CA1 synapse. Collectively, these data suggest that SEPTIN5 and its S327 phosphorylation status play a pivotal role in several cellular processes relevant for AD.

## 1. Introduction

Alzheimer's disease (AD), the most common form of dementia, is neuropathologically characterized by extracellular senile plaques containing amyloid-β (Aβ), intracellular neurofibrillary tangles composed of hyperphosphorylated tau protein (p-tau), and neuronal cell loss (Jack Jr et al., 2018). According to the prevailing amyloid cascade hypothesis, the pathogenesis of AD is initiated by abnormal accumulation of Aβ in the brain (Müller and Deller, 2017), followed by the aggregation of p-tau, leading to loss of synapses and neuronal cell death (Merluzzi et al., 2018). In AD, different isoforms of Aβ generated from the amyloid precursor protein (APP) owing to cleavage by β- and γ-secretases, are prone to aggregate in neurotoxic forms, triggering a cascade of events related to calcium dyshomeostasis, inflammation, oxidative stress, and synaptic dysfunction (Hardy and Selkoe, 2002). Indeed, increased levels of Aβ affect glutamatergic synaptic transmission, impairing long-term potentiation (LTP) (Snyder et al., 2005; Tackenberg et al., 2013), the molecular basis for learning and memory (Bliss and Collingridge, 1993).

Recently, septin family members, SEPTIN5 and SEPTIN8, were considered as new players in AD pathophysiology (Kurkinen et al., 2016; Marttinen et al., 2020). Although septins have been associated with other neurodegenerative diseases, such as Parkinson's disease, Huntington's disease, and frontotemporal dementia (Ageta-Ishihara et al., 2013; Czeredys et al., 2013; Gozal et al., 2011), the knowledge about the role of septins and their post-translational modifications (PTMs) in the cellular and synaptic dysfunction present in neurodegenerative disorders is elusive. The septin protein family members are a group of conserved guanosine-5-triphosphate binding proteins that are highly expressed in the brain and that have been highlighted as central components involved in the regulation of formation, growth and stability of axons and dendrites, synaptic plasticity, and vesicular trafficking (Amin et al., 2008; Ito et al., 2009; Marttinen et al., 2015; Mavrakis et al., 2014). Recent studies have identified SEPTIN5 and SEPTIN8 as potential modulators of APP processing and Aβ accumulation (Kurkinen et al., 2016; Marttinen et al., 2020). Specifically, mechanistic characterizations in neuronal cells have revealed that SEPTIN8 regulates the generation of Aβ *via* mechanisms altering the intracellular sorting and accumulation of β-site APP cleaving enzyme 1 (BACE1) (Kurkinen et al., 2016). Furthermore, the downregulation of SEPTIN5 resulted in increased autophagosomal degradation of APP C-terminal fragments (APP CTFs) as well as Aβ clearance in neuronal cells (Marttinen et al., 2020).

The existing data also highlight a central role for SEPTIN5 and SEPTIN8 in vesicle trafficking, docking, and release at presynaptic terminals through interaction with soluble N-ethylmaleimide-sensitive factor attachment protein receptor (SNARE) components known to regulate these processes, such as syntaxin-1 and synaptobrevin 2 (Beites et al., 2005; Ito et al., 2009; Taniguchi et al., 2007). Phosphorylation of SEPTIN5 in serine 327 (S327) decreases binding to syntaxin-1, and results in reduced stimulus-evoked secretion of human growth hormone in the rat pheochromocytoma PC12 cell line (Amin et al., 2008). Importantly, the S327 site is phosphorylated by cyclin dependent kinase 5 (CDK5) (Amin et al., 2008), whose activity is known to be upregulated in brain tissue from AD patients (Liu et al., 2016). However, whether SEPTIN5 levels are altered in AD and play a role in cellular and synaptic mechanisms affected in AD remains to be clarified.

Given these previous findings related to SEPTIN5, we set the focus on assessing RNA, protein and phosphopeptide levels of SEPTIN5 in *post-mortem* human temporal cortex with an increasing degree of AD-related neurofibrillary pathology. The total levels and S327 phosphorylation status of SEPTIN5 were also assessed in the cerebrospinal fluid (CSF) samples obtained from individuals fulfilling the criteria for mild cognitive impairment (MCI) due to AD. Further analyses were also performed to delineate the effects of SEPTIN5 S327 phosphorylation on APP processing, generation of Aβ, autophagy, neuronal survival, and inflammatory response upon basal and inflammation-induced conditions by transducing the different cortical mouse neuron models with the wild type SEPTIN5 (SEPTIN5 WT), non-phosphorylated SEPTIN5 mutant S327A (SEPTIN5 S327A), and phosphomimetic SEPTIN5 mutant S327D (SEPTIN5 S327D) lentiviral constructs. More specifically, aspartic acid is known to be chemically similar to phospho-serine and thus, we generated SEPTIN5 S327D mutant in the attempt to address the phosphorylation-specific effects of SEPTIN5 at the functionally relevant S327 site (Amin et al., 2008). Finally, to explore the effects of SEPTIN5 overexpression on synaptic function and its dependency on S327 phosphorylation and activity, mice were intrahippocampally injected with lentiviral SEPTIN5 WT, SEPTIN5 S327A and SEPTIN5 S327D constructs. After the behavioral assessments, *ex vivo* electrophysiological recordings in hippocampal slices were performed to evaluate both short- and long-term forms of synaptic plasticity using paired-pulse facilitation (PPF) and LTP protocols, respectively. Our results show that S327 phosphorylation levels of SEPTIN5 were significantly increased at the early stages of neurofibrillary pathology in human temporal cortex, but not in the CSF of MCI individuals due to AD. Additionally, the data suggest that the overexpression of SEPTIN5 alters processing of APP as well as autophagosomal activity in the mouse primary cortical neurons in a phosphorylation-dependent manner, while no effects on neuronal viability or neuroinflammatory responses in mouse neuron-BV2 microglial co-cultures upon induction of inflammation were observed. Overexpression of SEPTIN5 or its phosphomutants did not alter either cognitive performance or the *ex vivo* synaptic plasticity. However, SEPTIN5 S327D mutant resulted in decreased short-term plasticity relying on presynaptic mechanisms.

## 2. Materials and methods

### 2.1. Human neuropathological sample cohort

Basic characteristics and collection of human *post-mortem* temporal cortical samples, subsequent RNA and protein extractions as well as global transcriptomics, proteomics, and phosphopeptide analysis have been described in detail previously (Marttinen et al., 2019). Samples were classified according to Braak staging and grouped into four categories, as follows: stages 0 (RNA, $n = 6$; Protein & phosphopeptide, $n = 3$), stages I-II (RNA, $n = 22$; Protein & phosphopeptide, $n = 9$), stages III-IV (RNA, $n = 13$; Protein & phosphopeptide, n = 6), and stages V-VI (RNA, $n = 19$; Protein & phosphopeptide, $n = 18$) (Braak et al., 2006). Sample collection and use were approved by the Ethics Committee of Kuopio University Hospital, University of Eastern Finland, the Finnish National Supervisory Authority, and the Finnish Ministry of Social Affairs and Health (License number 362/06.01.03.01/2017).

### 2.2. Human CSF sample cohort

The dataset and samples used within this study are part of the *Beyond Beta Amyloid - Deciphering Early Pathogenic Changes in Alzheimer's disease* project (Fundação para a Ciência e Tecnologia, PTDC/MED-NEU/27946/2017). The project was approved by the local ethics committee and the participants provided their written informed consent. Participants were recruited at Memoclínica, a private memory clinic in Lisbon. Patients were individuals fulfilling the criteria for MCI due to AD - high likelihood - corresponding to the *highest level of certainty* (National

Institute on Aging - Alzheimer's Association workgroups, (Albert et al., 2011). The high likelihood requires clinical and cognitive criteria; biomarkers of Aβ deposition (low CSF Aβ1–42 levels or positive brain amyloid Pittsburgh B Compound Positron Emission Tomography (PET) scan); and biomarkers of neuronal injury (at least two positives: high CSF total tau or hyperphosphorylated tau, medial temporal lobe atrophy by volumetric measures or visual rating, temporoparietal hypometabolism by fluorodeoxyglucose PET imaging). Controls were subjects reporting cognitive complaints but showing none of the biomarkers of either Aβ deposition or neuronal injury, above indicated. Lumbar puncture (Engelborghs et al., 2017) and CSF handling (Teunissen et al., 2014) followed the established standard operating procedures. Briefly, after collection the samples were centrifuged at 2000*g* for 10 min at RT to pellet any cells or debris. Following centrifugation, CSF aliquots of 500 μl were stored in code-labelled polypropylene tubes at −80 °C until used for Western blot analysis.

### 2.3. Plasmid constructs, site-directed mutagenesis, and lentiviral packing

Plasmid DNA encoding wild type SEPTIN5 (RC206831L1, Origene) were used for site-directed mutagenesis using the QuikChange Lightning Site-Directed Mutagenesis kit (Agilent Technologies, Santa Clara, CA) according to the manufacturer's protocol. Shortly, forward, and reverse primers were designed to replace serine to alanine at the position 327 of SEPTIN5 (SEPTIN5 S327A) (5′-GATCGGGATGGGGGCCTC-CATGCGGCTG-3′ and 5′-CAGCCGCATGGAGGCCCCCATCCCGATC-3′) and serine to aspartate at the position 327 of SEPTIN5 (SEPTIN5 S327D) (5′-GGATCGGGATGGGGTCCTCCATGCGGCTGT-3′) and (5′-ACAGCCG-CATGGAGGACCCCATCCCGATCC-3′). One Shot TOP10 Competent *E. coli* cells were transformed with the generated PCR products and the transformed cells were plated on LB agar containing tetracycline, chloramphenicol, and ampicillin and kept at 37 °C overnight. Plasmids were extracted with QIAprep Spin Miniprep Kit (Qiagen) from viable colonies. Mutagenesis was confirmed by Sanger sequencing. Wild type SEPTIN5 (SEPTIN5 WT) and site-directed mutagenesis-generated SEPTIN5 S327A mutant and SEPTIN5 S327D without DDK-myc tag were cloned into the bicistronic pLVX EF1α-IRES-ZsGreen1 lentiviral expression vector (632,187, Takara, Mountain View, CA, USA) using PCR-cloning method. Third-generation self-inactivating lentiviruses were prepared in triple flasks by a calcium phosphate transfection method in 293 T cells as described previously (Follenzi and Naldini, 2002) and concentrated by ultracentrifugation.

### 2.4. Neuronal cultures and treatments

Mouse primary cortical neuronal cultures were prepared and cultured from embryonic day 18 JAXC57BL/6 J mice as previously described (Natunen et al., 2016). Lentiviral particles were introduced to the cortical neuron cultures at 10–20 multiplicity of infection at 5 *days in vitro* (DIV). Medium was changed 24 h after transductions, and cortical neurons cultures were cultured until 13 DIV. Mouse primary cortical neurons and BV2 microglia co-cultures were prepared as described before (Gresa-Arribas et al., 2012; Natunen et al., 2016). Briefly, BV2 cells were thawed and cultured in RPMI-1640-medium (Sigma) containing 10% fetal bovine serum, 2 mM L-glutamine and 100 U/ml penicillin and 100 μg/ml streptomycin, for two passages. RPMI-medium was replaced with neurobasal medium and BV2 cells were gently detached with a cell scraper. BV2 cells were added to the 11 DIV primary cortical neuron cultures in one-to-five ratio (BV2: neurons) and let settle down for two hours. Before establishing the co-cultures, mouse primary cortical neurons were transduced with control, SEPTIN5 WT, SEPTIN5 S327A, or SEPTIN5 S327D constructs at 5 DIV. Inflammation was induced by treating co-cultures with 200 ng/ml of lipopolysaccharide (LPS; Sigma) and 5 ng/ml of interferon-γ (IFNγ; Sigma) for 48 h, starting at 11 DIV.

### 2.5. Analysis of CSF samples

Protein concentration of all CSF samples was measured using the DC™ Protein Assay kit (Bio-Rad Laboratories, CA, USA), with bovine albumin serum (BSA) as standard. Samples were added to a mixture containing sample loading buffer, followed by heating for 10 min at 95 °C. Samples were run on 10% sodium dodecyl sulphate polyacrylamide gel electrophoresis, at constant voltage of 80–120 mV. Afterwards, proteins were transferred to polyvinylidene difluoride (PVDF) (GE Healthcare, UK) membrane, at 350 mA. Subsequently, PVDF membranes were stained with commercial Ponceau S solution (Sigma-Aldrich, USA), imaged, and then de-stained in ultrapure water. Membranes were blocked with 3% BSA in 1× Tris-buffered saline with Tween® 20 (TBS-T) for 1 h at RT, incubated in primary antibodies overnight, washed with TBS-T, incubated with secondary antibodies for 1 h at RT, and finally washed with TBS-T before visualize immunoreactivity using Amersham 680 systems (GE Healthcare, UK). The intensity of SEPTIN5 and SEPTIN5 S327 phosphoepitope bands were quantified by digital densitometry using ImageJ 1.45 software (Maryland, USA), and normalized to total protein-albumin, the most abundant CSF protein, previously used as loading control for CSF Western blot (Collins et al., 2015).

### 2.6. Western blot analysis of mouse primary cortical cultures

Total proteins were extracted from mouse primary cortical neurons using transmembrane protein extraction reagent buffer (Pierce) containing 1:100 diluted protease and phosphatase inhibitors (Thermo Scientific). Protein concentrations were measured using bicinchoninic acid assay (Pierce). Ten to 50 μg of total protein lysates were separated using 4–12% bis-Tris polyacrylamide gel electrophoresis (PAGE; Invitrogen) and subsequently transferred to PVDF membrane (GE Healthcare, UK). Non-specific antibody binding was prevented by incubating PVDF membrane in blocking solution containing 5% non-fat milk in 1× TBST for 1 h at RT. Protein detection from the PVDF membrane was performed with specific primary antibodies diluted appropriately in 1× TBS-T and incubated overnight at 4 °C. This was followed by 1 h incubation with secondary anti-mouse or anti-rabbit antibodies, conjugated with horseradish peroxidase (HRP), diluted in 1× TBS-T, for 1 h at RT. Enhanced-chemiluminescence substrate (GE Healthcare) was evenly applied on the top of the membrane and subsequently protein bands were detected with Syngene Gbox or Chemidoc MP imaging system, and intensities quantified using Quantity One or ImageLab (Bio-Rad) software.

### 2.7. Antibodies used for the Western blot analyses

SEPTIN5 was recognized by anti-SEPTIN5 polyclonal antibody (1:1000, 11,631–1-AP; ProteinTech Group). The phospho-specific SEPTIN5 anti-Ser(P)327 antibody was kindly provided by Dr. Niranjana D. Amin, originally produced by Cedarlane Laboratories (Burlington, NC) (Amin et al., 2008). The antibody binds sequence KLTQDSRMES (PO4) PIPILPL. BACE1 protein was detected by rabbit monoclonal anti-BACE1 D10E5 antibody (1:1000, #5606; Cell Signaling Technology). Rabbit polyclonal antibody recognizing APP C-terminus (1:2000, A8717; Sigma) was used to detect APP immature (APPim), APP mature (APPm), and APP CTFs (C83 and C99). Soluble sAPPα and sAPPβ were detected from cell culture media using a mouse monoclonal antibody (6E10, Biosite) and a specific in-house rat monoclonal antibody (BAWT) generated against amino acids 11–16 of Aβ (a kind gift from Prof. Stefan Lichtenthaler, DZNE, Munich, Germany), respectively. Total sAPP (sAPPtot = sAPPα + sAPPβ) levels were detected from cell culture media using a mouse monoclonal antibody recognizing the N-terminus of APP (MAB348, clone 22C11; Millipore). LC3I and LC3II were detected using anti-LC3B rabbit polyclonal antibody (1:3000, ab51520; Abcam). p62 protein was detected using a rabbit polyclonal antibody (1:1000,

ab76340; Abcam). β-actin was recognized by a mouse monoclonal antibody (1:1000, ab8226; Abcam).

### 2.8. Aβ measurements from medium samples

Aβ40 and Aβ42 levels were measured from mouse primary cortical neuron cell culture medium using Human/Rat β Amyloid 40 (294–64,701) ELISA Kit (Wako) and β Amyloid 42 (High-Sensitive; 292–64,501) ELISA Kit (Wako) according to manufacturer's protocol.

### 2.9. Neuronal viability and TNF-α assays

Mouse primary cortical neurons and BV2 microglia co-cultures were fixed in 4% paraformaldehyde for 20 min at RT and rinsed twice with phosphate-buffered saline (PBS). Cells were permeabilized in methanol containing 0.3% $H_2O_2$ for 10 min and subsequently blocked with blocking solution (PBS, 1% BSA and 10% horse serum, Vector Labs) for 20 min at RT. Neuronal cells were stained with anti-MAP2 primary antibody (1:2000; Sigma, M9942) overnight at 4 °C. Next day, cells were washed three times with PBS and incubated for 1 h with biotinylated horse anti-mouse secondary antibody (1:200; Vector Labs), followed by three washes and ExtrAvidin®-HRP tertiary antibody staining (1:500; Sigma) for 1 h at RT. After tertiary antibody incubation cells were again washed three times with PBS. To develop the color, cells were incubated with the ABTS peroxidase substrate kit (Vector Labs) according to the manufacturer's instructions in the dark for 30 min. From each well, 150 µl of substrate solution was transferred to fresh 96-well plate and absorbances were measured at 405 nm with enzyme-linked immunosorbent assay (ELISA) microplate reader (BioRad). The levels of secreted tumor necrosis factor alpha (TNF-α) from conditioned culture media were measured using an ELISA kit (Ready-set-go mouse-TNF-α, eBioscience) according to the manufacturers' instructions. Absorbances from two-fold diluted medium samples were measured at 450 nm using an ELISA microplate reader (BioRad).

### 2.10. Animals

Mice used for the behavioral assessment, immunohistochemistry and electrophysiological studies were male C57BL/6 J mice (8 to 10 weeks old; Charles River, Barcelona, Spain). Animal maintenance and experimental procedures were performed in accordance with the EU Directive 2010/63/EU, Portuguese law on animal care (*Decreto-Lei* 113/2013) and approved by the Instituto de Medicina Molecular João Lobo Antunes Internal Committee and the Portuguese Animal Ethics Committee (Direcção Geral de Veterinária).

### 2.11. Stereotaxic surgery for in vivo lentiviral delivery

Mice were randomized into four groups to receive the lentiviral vectors: control (ctrl)-pLVX, empty viral vector; SEPTIN5 WT-pLVX, SEPTIN5 wild type; SEPTIN5 S327A-pLVX, SEPTIN5 S327A phosphomutant cDNA; and SEPTIN5 S327D-pLVX, SEPT5 S327D phosphomimetic cDNA. Mice were bilaterally injected with 1 µl of the respective viral constructs, at the following coordinates: - 1.9 AP, ± 2.2 ML, − 2 DV, targeting the CA3 area of the hippocampus. Lentiviral transduction developed for five to six weeks, after which mice were, tested behaviorally (Fig. S1).

### 2.12. Behavioral assessments

Mice were handled for five days prior to behavioral tests. Open field (OF) and Morris water maze (MWM) tests were recorded using the SMART V2.5 video-tracking software (PanLab, Barcelona, Spain), while Y-maze spontaneous alternation (SA) and elevated-plus maze (EPM) tests were video recorded for later analysis. The OF test appraises locomotor and exploratory activity (Prut and Belzung, 2003). Without prior habituation, mice were individually positioned in the center of an empty square arena surrounded by walls (60x60x40 cm), virtually divided in three concentric squares at a similar distance from each other. The total distance traveled, and time spent in the center *versus* in periphery of the arena were recorded for 5 min. EPM test was used to evaluate anxiety-related behavior (Walf and Frye, 2007). Without prior habituation, mice were individually placed in the intersection of a plus-shape maze elevated 50 cm above the floor, comprising two well-lit open arms (50 × 10 cm) and two dark enclosed arms (50x10x30 cm). The number of total transitions and the time spent inside open-closed arms were video-recorded for 5 min. Spatial working memory was assessed using the spontaneous alternation version of the Y-maze test (Hughes, 2004; Spellman et al., 2015). Without prior habituation, animals were individually positioned at the start arm of the Y-shaped maze, composed by three identical arms (each with 15x5x12 cm), converging to an equal angle (120°). For each animal, spontaneous alternation was scored as the number of consecutive entries without arm repetition (EWR) to the total number of three sequential arm entries performed (EP) minus 2: [(number of EWR)/(number of EP-2)*100], during 5 min. Hippocampal-dependent spatial learning and memory was evaluated by the MWM test (Vorhees and Williams, 2006), as previously described (Batalha et al., 2013; Batalha et al., 2016). The water maze consisted of a circular pool (100 cm diameter, 60 cm height), filled with white opaque water at RT (24 ± 1 °C). The poll was virtually divided into four quadrants. An escape platform (8 cm diameter) was placed in the center of the target quadrant, beneath water surface. Visual cues were positioned on the walls of the testing room. During the learning phase, animals were tested for four consecutive days with four swimming trials per day (30 min inter-trial interval). Each trial had a maximum of 60 s for the animal to find the platform and remain on top of it for at least 10 s. One day after completion of the learning phase, a probe test was conducted, consisting of a single trial of 60 s in which the platform was removed, and the time each animal spent searching for the platform in the target quadrant was recorded.

### 2.13. Acute hippocampal slice preparation

Mice were deeply anesthetized with isoflurane and sacrificed by decapitation. The brain was rapidly removed, and the hippocampi were dissected in ice-cold artificial cerebrospinal fluid (aCSF) solution containing: 124 mM NaCl, 3 mM KCl, 1.2 mM $NaH_2PO_4$, 25 mM $NaHCO_3$, 2 mM $CaCl_2$, 1 mM $MgSO_4$, and 10 mM glucose, pH 7.4, previously gassed with 95% $O_2$ and 5% $CO_2$. Transverse hippocampal slices of 400 µm thickness were cut using a McIlwain tissue chopper. Lentiviral transduction was confirmed in all hippocampal slices, by the presence of the ZsGreen1 fluorescent protein (ZsGreen1 +), using Axiovert 200 inverted widefield fluorescence microscope (Carl Zeiss Inc., Göttingen, Germany), with a 5× objective. Images were acquired using the software AxioVision 4 (Carl Zeiss Inc.). ZsGreen1+ slices were kept at RT, in a chamber continuously superfused with gassed aCSF, to recover functional and energetically.

### 2.14. Electrophysiological recordings

Individual slices were transferred to a chamber continually perfused with gassed (95% $O_2$ and 5% $CO_2$) aCSF solution, at a constant flow rate of 3 ml/min and temperature of 32 °C. Field excitatory postsynaptic potentials (fEPSPs) were elicited by rectangular pulses of 0.1 ms duration, delivered every 20 s, using a bipolar concentric electrode (Harvard) placed in the Schaffer collaterals/commissural fibers of the CA1 area of the hippocampus. Averages of six consecutive individual recordings were acquired in the *stratum radiatum* of the CA1 area, using a glass micropipette (2–6 MΩ resistance) filled with oxygen-saturated aCSF solution. Data acquisition and re-analysis were performed using WinLTP software. Capabilities of the WinLTP data acquisition program extending beyond basic LTP experimental functions (Anderson and

Collingridge, 2007). All protocols were started after a stable baseline of at least 10 min. PPF was assessed by delivering two sequential stimulation pulses at four different inter-pulse intervals (20 to 100 ms). PPF was measured as the ratio between the fEPSP slope of the second evoked stimulus *versus* the fEPSP slope of the first stimulus (S2/S1). Synaptic efficiency was assessed using a standard input/output (I/O) curves protocol. Stimulus was consecutively increased in 20 μA steps, from 60 μA to a maximum intensity of 320 μA. The I/O curves are represented as the fEPSP slope *versus* percentage of stimulation, where 0% stimulation is the stimulus intensity that starts to elicit a measurable fEPSP response, and 100% stimulation the stimulus intensity that elicits a maximum fEPSP response, for each hippocampal slice. Post-tetanic potentiation (PTP) was evaluated in the first four minutes following the delivery of theta-burst ($\theta$-burst) protocol to induce LTP. $\theta$-burst consisted of four trains with four pulses of 100 Hz each, with 200 ms intertrain interval. The magnitude of PTP was calculated as the percentage of change in fEPSP slopes normalized to baseline fEPSP. The magnitude of LTP was calculated as percentage change in fEPSP slopes after 50–60 min of $\theta$-burst stimulation normalized to baseline fEPSP.

### 2.15. Histological procedures

Mice were deeply anesthetized with isoflurane and transcardially perfused with PBS, followed by 10% formalin neutral buffer solution (Sigma). Brains were removed, post-fixed for 24 h in 10% formalin, cryoprotected in 15% followed by 30% sucrose solution, and embedded in gelatin, prior to isopentane freezing at −70 °C. For fluorescence analysis, coronal sections of 50 μm thickness were incubated with 4′,6-diamidino-2-phenylindole, washed once, and mounted in Dako fluorescent mounting medium (Agilent Technologies, USA). Hippocampal images were acquired using a Zeiss LSM 880 (Carl Zeiss, Oberkochen, Germany) confocal microscope, with a 20× objective.

### 2.16. Statistical analysis

GraphPad Prism 8.0, IBM SPSS version 21 or R was used to analyze the data. Results are expressed as means ± standard error of the mean (SEM). *P-values* ($p$) <0.05 were considered statistically significant. Statistical comparisons of results obtained in experiments were performed by independent samples *t*-test for two-group comparisons. A comparison of three or more groups was performed using one-way ANOVA followed by Tukey honest significant difference (HSD) or Fisher's least significant difference (LSD) *post hoc* test. PPF and I/O curves statistical analyses were performed using repeated-measures ANOVA. The four animal groups (ctrl-pLVX, SEPTIN5 WT-pLVX, SEPTIN5 S327A-pLVX and SEPTIN5 S327D-pLVX) were considered to represent between-subject effects, while the interpulse intervals or stimulus intensities were considered within-subject effects. *Post hoc* differences were evaluated with the Tukey HSD test.

## 3. Results

### 3.1. RNA, protein, and phosphopeptide levels of SEPTIN5 are altered in the human temporal cortical samples with different stages of AD-related neurofibrillary pathology

We have recently shown that the downregulation of SEPTIN5 resulted in the increased autophagosomal degradation of APP C-terminal fragments as well as Aβ clearance in neuronal cells both in *in vitro* and *in vivo* (Marttinen et al., 2020). To further assess the relationship

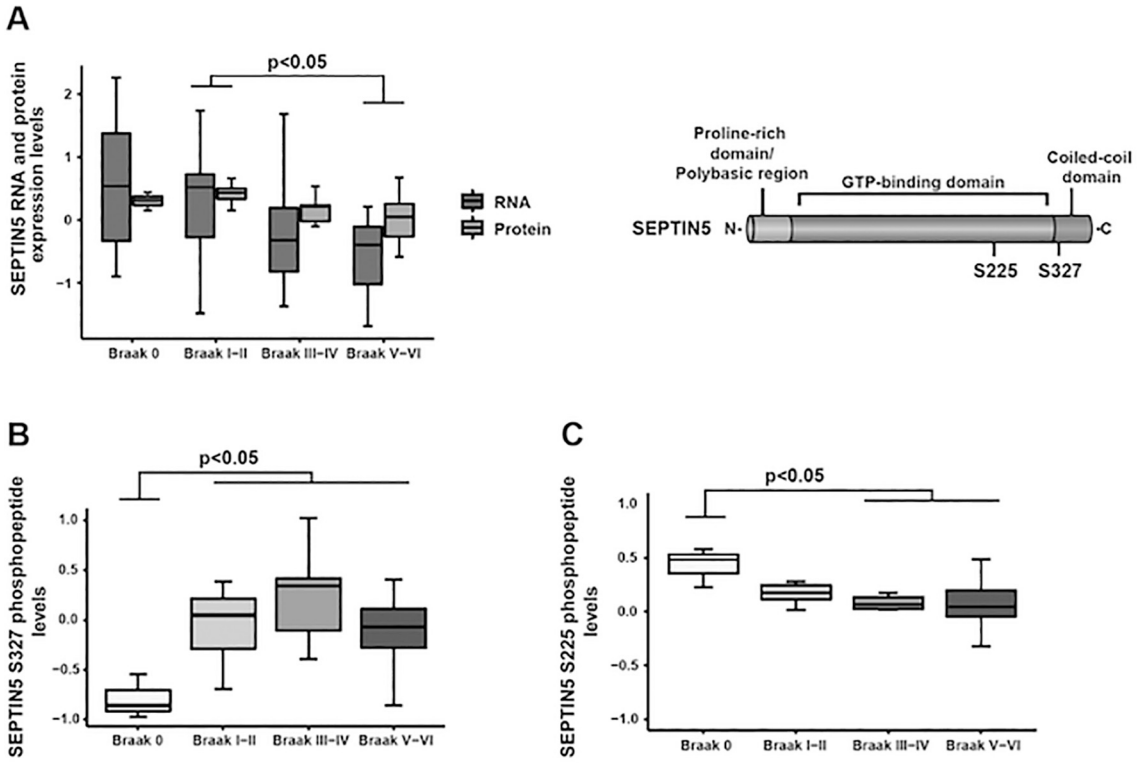


**Fig. 1.** RNA, protein and phosphopeptide levels of SEPTIN5 are significantly altered in the human temporal cortex with respect to increasing neurofibrillary pathology. A) RNA and protein levels of SEPTIN5 were significantly decreased in the later stages of AD-related neurofibrillary pathology. B) The levels of SEPTIN5 S327 phosphoepitope showed a significant increase in the early stages of AD-related neurofibrillary pathology. C) The levels of SEPTIN5 S225 phosphoepitope are significantly decreased in the advanced Braak stages (III-VI) as compared to samples without neurofibrillary pathology (Braak stage 0). $n$ = 36–60 (RNA: Braak 0, $n$ = 6; Braak I-II, $n$ = 22; Braak III-IV, $n$ = 13; Braak V-VI, $n$ = 19. Protein & phosphopeptide: Braak 0, n = 3; Braak I-II, $n$ = 9; Braak III-IV, $n$ = 6; Braak V-VI, $n$ = 18). Box plots showing the median, 25th and 75th percentiles, error bars show 1.5 interquartile ranges. ANOVA *post hoc* Tukey HSD.

between SEPTIN5 and AD-related alterations, we analyzed the levels of RNA (microarray-based data), protein (LC-MS/MS-based data), and functionally relevant phosphorylation sites (S225 and S327, LC-MS/MS-based data) of SEPTIN5 in well-characterized human *post-mortem* temporal cortical tissue samples with respect to increasing degree of AD-related neurofibrillary pathology (Braak stages 0-VI) (Fig. 1A) as described previously (Marttinen et al., 2019). We found a significant decrease in the RNA and protein levels of SEPTIN5 in the late stages of neurofibrillary pathology (Braak stages V and VI) as compared to the early-stage samples (Braak stages I and II, but not Braak stage 0). Conversely, a significant increase in the S327 phosphoepitope levels of SEPTIN5 was detected already in the Braak stages I and II as compared to samples without neurofibrillary pathology (Braak stage 0, Fig. 1B). Conversely, S225 phosphoepitope levels of SEPTIN5 showed a significant decrease in relation to the advanced stages of neurofibrillary pathology (Braak stages III), potentially reflecting the observed decrease in the total protein levels of SEPTIN5. We next assessed CSF samples obtained from individuals with MCI due to AD and individuals with cognitive complaints but no biomarkers for Aβ deposition or neuronal injury (control group) using Western blot with anti-SEPTIN5 and phospho-specific SEPTIN5 anti-Ser(P)327 antibodies, respectively (Fig. 2). No significant differences were observed in the levels of SEPTIN5 ($p > 0.05$, independent samples *t*-test, $n = 20$–24), in the phosphorylation status of SEPTIN5 S327 ($p > 0.05$, independent samples t-test, $n = 10$–11), or the ratio of SEPTIN5 S327/SEPTIN5 between MCI due to AD and control groups. To determine whether the total levels of SEPTIN5 and the phosphorylation status of S327 were altered in relation to age, we assessed the levels in the hippocampus of aged rats presenting initial cognitive decline (Pinho et al., 2017). No significant differences were detected between the two age groups ($p > 0.05$, independent sample t-test, $n = 6$, Fig. S1). Collectively, these data suggest significant alterations in the RNA, protein and phosphoepitope levels of SEPTIN5 with respect to the increasing degree of AD-related neurofibrillary pathology in human brain, warranting further mechanistic investigations of the role of SEPTIN5 and its phosphorylation-related PTMs in the cellular processes relevant for AD.

### 3.2. *SEPTIN5 alters the APP processing in S327 phosphorylation-dependent manner in mouse primary cortical neurons*

Next, we aimed to understand the consequences of the observed significant increase in SEPTIN5 S327 phosphorylation in the human temporal cortex in relation to AD-related neurofibrillary pathology. First, we transduced mouse primary cortical neurons with SEPTIN5 WT-pLVX construct to assess the effects of SEPTIN5 overexpression on APP processing and Aβ generation. A 2.5-fold increase in SEPTIN5 expression was observed in SEPTIN5 WT-transduced cortical neurons as compared to control neurons (Fig. 3A). In contrast to the previously shown effects of SEPTIN5 downregulation on APP and Aβ metabolism in mouse primary cortical neurons (Marttinen et al., 2020), the overexpression of SEPTIN5 WT resulted in a significant increase in the ratio of mature/immature APP isoforms (APPm/im) and in the levels of BACE1 accompanied with a minor increase in the levels of APP C-terminal fragments (APP CTF) (Fig. 3A). Analysis of culture medium samples obtained from the mouse primary cortical neurons did not reveal significant changes in the levels of Aβ40, Aβ42, sAPPα, sAPPβ, sAPPtot, or the ratio of Aβ42/Aβ40 upon the overexpression of SEPTIN5 WT (Fig. 3B). As the downregulation of SEPTIN5 was shown to be linked to increased autophagosomal degradation of APP C-terminal fragments and Aβ (Marttinen et al., 2020), we next assessed the effects of SEPTIN5 WT overexpression on key autophagosomal proteins by assessing the levels of LC3 and p62 from the protein lysates (Fig. 3C). The overexpression of SEPTIN 5 WT led to a significant ~1.8-fold increase in the protein levels of LC3II, while the protein levels of LC3I and the ratio of LC3II/I revealed a trend towards increase, which did not reach statistical significance. The levels of autophagy-associated receptor p62 remained unchanged upon the overexpression of SEPTIN5 WT construct. To specifically elucidate the functional relevance of SEPTIN5 S327 phosphorylation in these above-mentioned cellular processes related to APP processing and autophagy, we generated a phosphodeficient SEPTIN5 S327A (SEPTIN5 S327A-pLVX) and phosphomimetic SEPTIN5 S327D (SEPTIN5 S327D-pLVX; chemically similar to phospho-serine) mutants *via* site-directed mutagenesis, which were inserted into a lentiviral vector. Western blot analysis of SEPTIN5 S327A- and SEPTIN5 S327D-transduced cortical neurons showed a ~ 2-fold increase in the levels of SEPTIN5, but unchanged SEPTIN5 S327 phosphorylation levels using a SEPTIN5 phospho-S327-specific antibody as compared to neurons transduced with control lentivirus (Fig. 3A). Transduction of mouse primary cortical neurons with the SEPTIN5 S327A mutant did not reveal any statistically significant changes in the protein lysate or medium samples in terms of APP processing-related parameters (Fig. 3A and B). Furthermore, the observed increase in the protein levels of LC3II upon the overexpression of SEPTIN5 WT was not detected in SEPTIN5 S327A-transduced mouse primary cortical neurons (Fig. 3C). Conversely, SEPTIN5 S327D mutant

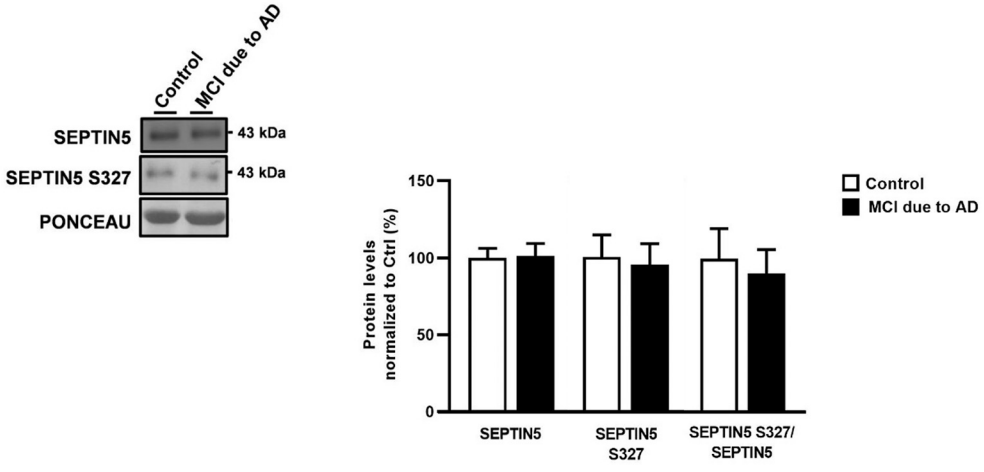


**Fig. 2.** The levels of SEPTIN5 and SEPTIN5 S327 phosphoepitope in the CSF samples obtained from individuals with MCI due to AD and individuals with cognitive complaints but showing no biomarkers for Aβ deposition or neuronal injury. Representative western blot and quantification of the protein levels of SEPTIN5, SEPTIN5 S327, and the ratio of SEPTIN5 S327/SEPTIN5. Protein levels were normalized to total protein using red Ponceau S staining of membrane-adsorbed albumin and are shown as % of control. $n = 10$–24 (SEPTIN5: control, $n = 20$; MCI due to AD $n = 24$. SEPTIN5 S327: control, $n = 11$; MCI due to AD, n = 10). Note that controls are individuals with cognitive complaints but showing no biomarkers for Aβ deposition or neuronal injury. MCI due to AD individuals have positive biomarkers of Aβ deposition and biomarkers of neuronal injury, according to the NIA-AA criteria (Albert et al., 2011). Mean ± SEM; independent samples *t*-test; $p > 0.05$. (For interpretation of the references to color in this figure legend, the reader is referred to the web version of this article.)

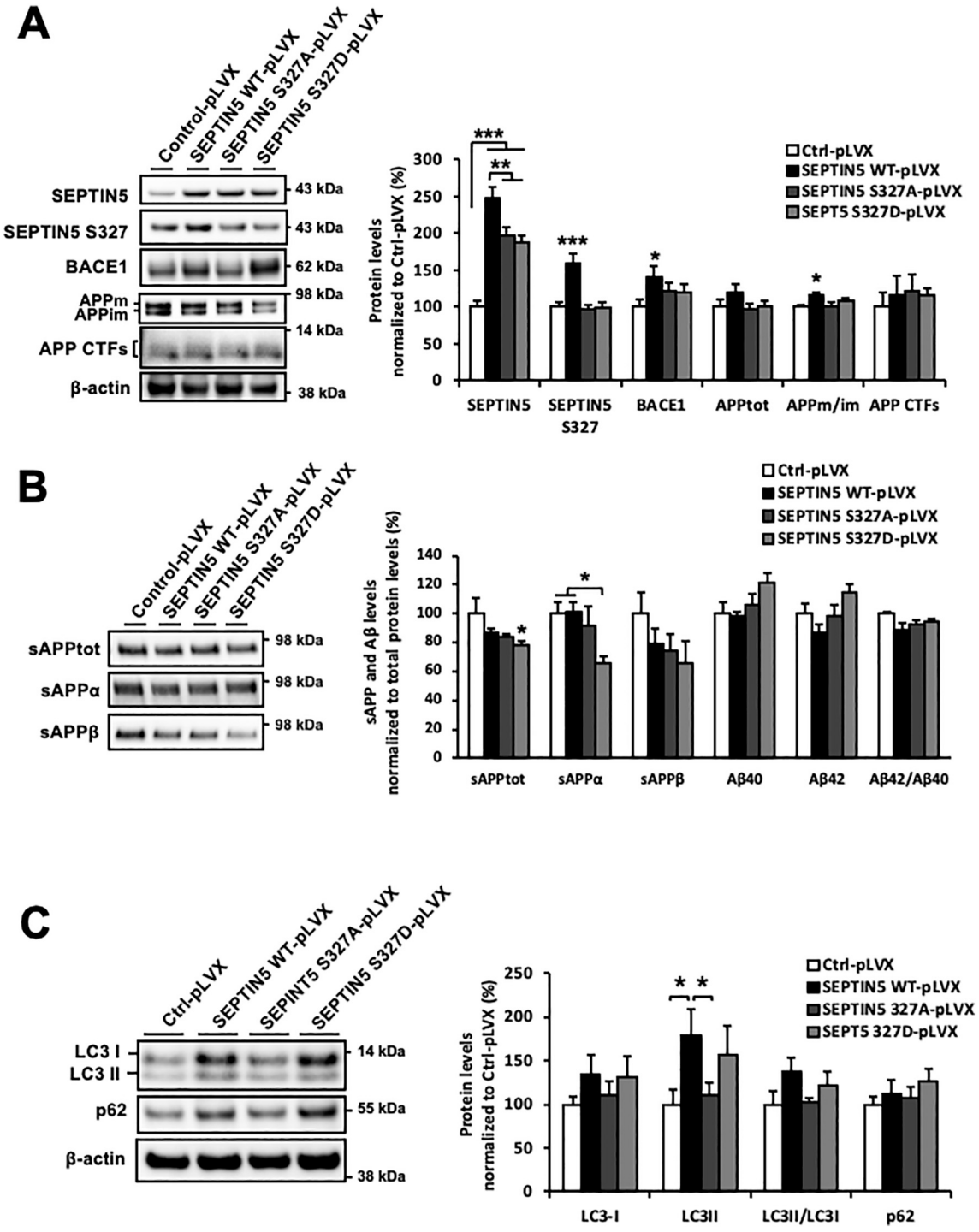


**Fig. 3.** Overexpression of SEPTIN5 significantly alters APP processing and the levels of LC3II in the primary mouse cortical neurons in a S327 phosphorylation-dependent manner. A) Western blot analysis showing a significant overexpression of SEPTIN5 wild type and phosphomutants in mouse primary cortical neurons transduced with control (Ctrl-pLVX), SEPTIN5 wild type (SEPTIN5 WT-pLVX), SEPTIN5 S327A (SEPTIN5 S327A-pLVX), and SEPTIN5 S327D (SEPTIN5 S327D-pLVX) lentiviral constructs. The overexpression of SEPTIN5 wild type, but not phosphomutants affected the APP processing-related parameters, n = 3–6. B) Analysis of culture medium samples obtained from the mouse primary cortical neurons in terms of Aβ40, Aβ42, sAPPα, sAPPβ, sAPPtot, and the ratio of Aβ42/Aβ40 upon the overexpression of SEPTIN5 wild type or phosphomutants, $n = 6$. C) Western blot analysis of autophagosomal proteins LC3 and p62 from the protein lysates extracted from the mouse primary cortical neurons upon the overexpression of SEPTIN5 wild type or phosphomutants. LC3II expression was significantly increased in SEPTIN5 wild type overexpressing samples as compared to control samples, n = 6. In A and C, protein levels were normalized to β-actin and are shown as % of Ctrl-pLVX. In B, the levels were normalized to total protein levels in the respective cell lysates and are shown as % of Ctrl-pLVX. Mean ± SEM, One-way ANOVA, *post hoc* LSD; * $p < 0.05$, ** $p < 0.01$, *** $p < 0.001$.

caused a significant decrease in the culture medium levels of sAPPα and sAPPtot without any changes in terms of APP processing-related parameters in the protein lysates (Fig. 3A and B). However, it should be noted that a non-significant decrease in the medium levels of sAPPtot was also observed in SEPTIN5 WT- and S327A-transduced cortical neurons, indicating that the decrease in the levels of sAPPα was not only observed in SEPTIN5 S327D-transduced neurons. Interestingly, overexpression of SEPTIN5 S327D mutant showed a trend towards an increase in the levels of LC3II similar to that observed with the SEPTIN5 WT (Fig. 3C). Collectively, these data suggest that the overexpression of SEPTIN5 alters APP processing and the levels of autophagy-related LC3II protein in mouse primary cortical neurons in a S327 phosphorylation-dependent manner.

### 3.3. Overexpression of SEPTIN5 wild type or SEPTIN5 phosphomutants do not affect neuronal viability or inflammatory responses in mouse neuron-BV2 microglial co-cultures upon the induction of inflammation

To test whether the overexpression of SEPTIN5 and its altered S327 phosphorylation status affect neuronal viability or inflammatory responses upon LPS and IFNγ-induced inflammation, SEPTIN5 WT and SEPTIN5 phosphomutant constructs were expressed in a well-established primary mouse cortical neuron-BV2 microglia co-culture model (Gresa-Arribas et al., 2012; Natunen et al., 2016). In line with neuronal monoculture data (Fig. 3A), a ~ 2-fold increase in the neuron-derived expression of SEPTIN5 WT and mutants was observed in the co-cultures (Fig. 4A). Similar to the downregulation of SEPTIN5 in the neuron-BV2 microglia co-culture model (Marttinen et al., 2020), the overexpression of SEPTIN5 WT or SEPTIN5 phosphomutants did not alter neuronal viability or TNFα production in the vehicle- or LPS and IFNγ-treated co-cultures (Fig. 4B and C). Taken together, these data suggest that the overexpression of SEPTIN5 WT or SEPTIN5 phosphomutants do not affect neuronal viability or inflammatory responses in mouse neuron-BV2 microglial co-cultures upon the induction of AD-related inflammation.

### 3.4. Overexpression SEPTIN5 wild type or SEPTIN5 phosphomutants in the hippocampus of mice do not affect behavioral readouts

One of the earliest symptoms of AD is cognitive decline. To evaluate the impact of SEPTIN5 phosphorylation on cognition, C57BL/6 animals were intrahippocampally injected with lentiviral ctrl-pLVX, SEPTIN5 WT-pLVX, SEPTIN5 S327A-pLVX, and SEPTIN5 S327D-pLVX constructs. Five to six weeks after surgery, animals were subjected to a battery of

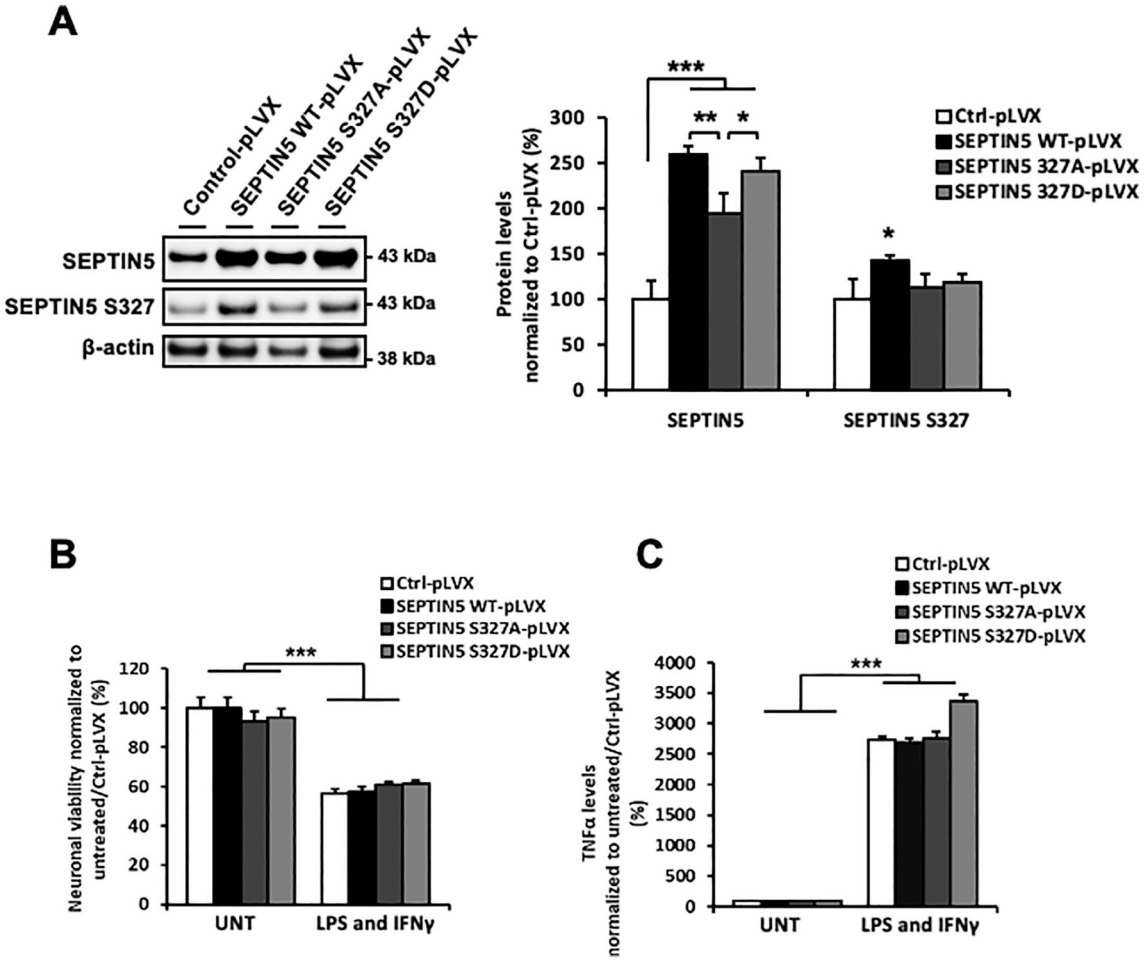


**Fig. 4.** Overexpression of SEPTIN5 wild type or SEPTIN5 phosphomutants do not affect neuronal viability or inflammatory response in the mouse primary cortical neuron-BV2 microglia co-cultures. A) Western blot analysis showing a significant increase in the levels of SEPTIN5 wild type and phosphomutants in neuron-BV2 cell co-cultures upon vehicle conditions. Phosphorylation status of S327 site was assessed using the phospho-specific SEPTIN5 anti-Ser(P)327 antibody. Protein levels were normalized to β-actin and are shown as % of Ctrl-pLVX. B) Neuronal viability was significantly decreased after LPS and IFNγ-treatment as compared to the untreated (UNT) co-cultures. Neuronal viability was unaltered due to the overexpression of SEPTIN5 wild type or phophomutants in both untreated or LPS and IFNγ-treated co-cultures. C) TNF-α levels were significantly increased upon treatment with LPS and IFNγ as compared to untreated co-cultures. Overexpression of SEPTIN5 wild type or phosphomutants did not alter the levels of TNF-α in the untreated or LPS and IFNγ-treated co-cultures as compared to control co-cultures, $n = 4$, mean ± SEM, One-way ANOVA, *post hoc* LSD, ** $p < 0.01$, *** $p < 0.001$.

behavioral tests (Fig. S2). Locomotor and general exploratory behaviors were assessed using the OF test. No differences in the total distance traveled, and in time spent in central *versus* peripheral zones were observed among the groups ($p > 0.05$, one-way ANOVA, $n = 10–14$, Fig. 5A-I and A-II, respectively). In a similar way, no differences among the groups were observed in anxiety-related behavior, evaluated using the EPM test ($p > 0.05$, one-way ANOVA, n = 10–14, Fig. 5B-I and B-II). Hippocampal-related functions were assessed using the spontaneous alternation Y-maze test for short-term working memory, and the MWM test for long term memory and learning. No differences in short-term memory were found among the groups, with a similar number of spontaneous alternations in the Y-maze test, measured by the alternation index ($p > 0.05$, one-way ANOVA, n = 10–14, Fig. 5C-I). In the MWM test, all groups showed a similar latency to the target during the four training days of the learning phase ($p > 0.05$, one-way ANOVA, $n = 5–8$, Fig. 5D-I), and similar time spent in the target quadrant during the probe test ($p > 0.05$, one-way ANOVA, n = 5–8, Fig. 5D-II). After behavioral assessment, two animals from each group were used to prepare coronal brain sections to confirm SEPTIN5 expression through the presence of the ZsGreen1 fluorescent protein. In general, all analyzed coronal sections displayed intense ZsGreen1 signal mostly in the DG and the *stratum lucidum* of the CA3 areas of the hippocampus. In some sections in all groups, CA1 pyramidal cells also expressed ZsGeen1 fluorescent protein (Fig. S3). Collectively, these data suggest that the overexpression of SEPTIN5 WT or SEPTIN5 phosphomutants do not affect cognitive performance of C57BL/6 mice.

### 3.5. S327 phosphorylation of SEPTIN5 alters short-term synaptic plasticity

Considering the proposed role of SEPTIN5 in the regulation of vesicle fusion that enables neurotransmitter release at the presynaptic membrane, we performed *ex vivo* electrophysiological recordings in hippocampal slices prepared from the animals after behavioral testing. Hippocampal slices from each condition were selected after the confirmation of ZsGreen1 fluorescence (Fig. S4). We used a paradigm that exclusively relies on presynaptic mechanisms (paired-pulse stimulation) to measure presynaptic changes in the release probability. All groups displayed PPF across the different interstimulus intervals (20, 50, 70, 100 ms). *Post hoc* analysis revealed that PPF ratio in hippocampal slices overexpressing SEPTIN5 S327D-pLVX was significantly reduced when compared to SEPTIN5 S327A-pLVX ($p < 0.05$, repeated-measures ANOVA, *post hoc* Tukey HSD, n = 5–9, Fig. 6B). I/O curves were also recorded from the Schaffer collateral-commissural fibers of the hippocampus to assess alterations in basal synaptic efficiency. As expected, higher stimulus intensities evoked significantly larger fEPSP slopes. However, neither differences among the groups nor significant interactions between the groups and stimulus intensities were observed ($p > 0.05$, repeated-measures ANOVA, $n = 4–9$, Fig. 6C). Since SEPTIN5 has been associated to synaptic modulation (Marttinen et al., 2015), and one of the early manifestations of AD is disruption of synaptic plasticity, we evaluated LTP. The magnitude of LTP was not different among the groups ($p > 0.05$, one-way ANOVA, $n = 6–9$, Fig. 6F). However, despite

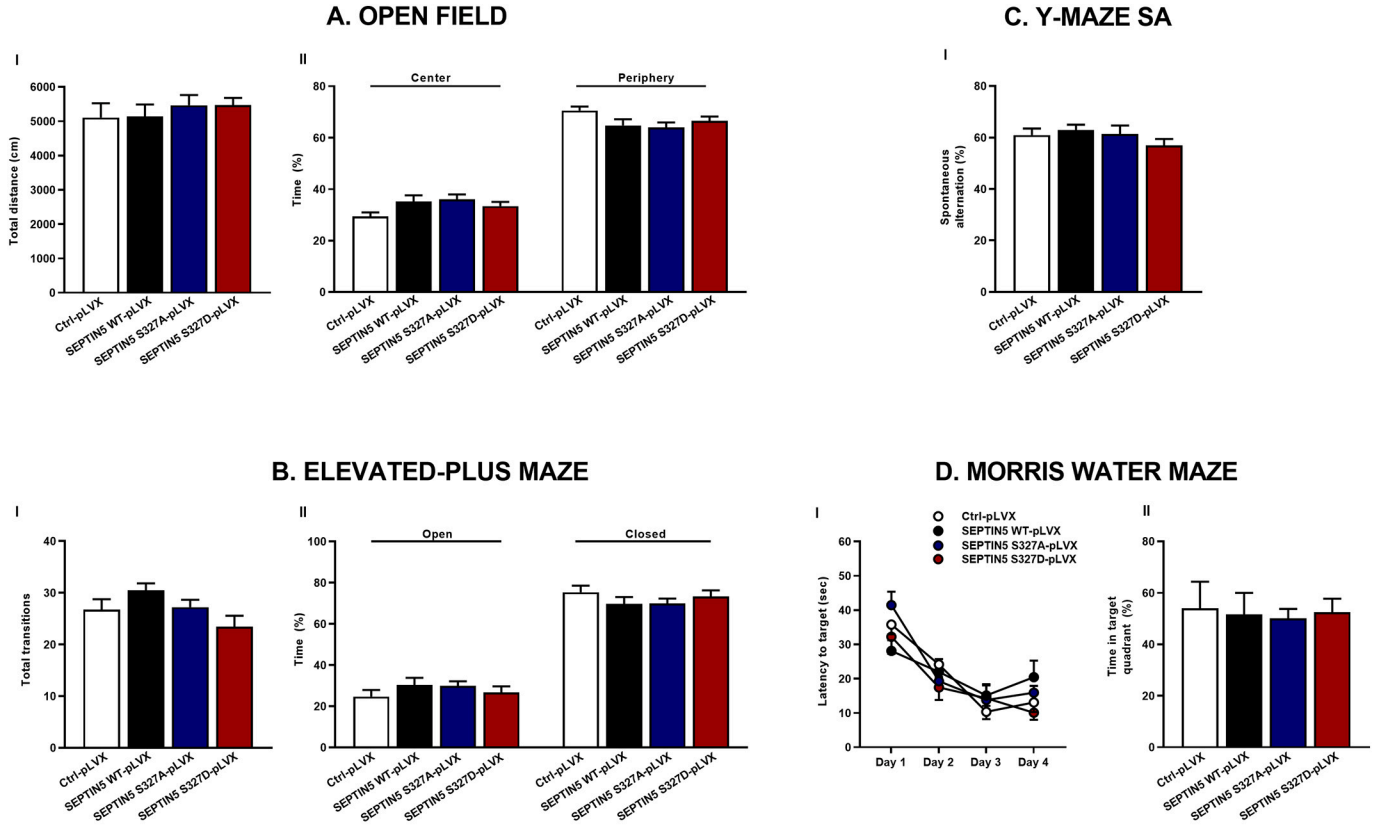


**Fig. 5.** Behavioral analysis to characterize the cognitive performance of mice intrahippocampally injected with lentiviral ctrl-pLVX, SEPTIN5 WT-pLVX, SEPTIN5 S327A-pLVX and SEPTIN5-S327D-pLVX constructs. A) Open field test: Locomotor and exploratory activity were evaluated as total distance traveled (cm) (I), and percentage of time spent in the center *versus* periphery of the arena (II). B) Elevated-plus maze test: Anxiety-related behavior was measured as total entries (I), and percentage of time spent in open *versus* closed arms (II). C) Y-maze spontaneous alternation test: Spatial working memory was evaluated by measuring the percentage of spontaneous alternations between the three arms of the maze (I). D) Morris water maze: Learning curves during the four trial days (I), and percentage of time spent in the target quadrant (II). $n = 5–14$ (Open Field, Elevated-plus maze, and Y-maze spontaneous alternation tests: ctrl-pLVX, n = 11; SEPTIN5 WT-pLVX, n = 10; SEPTIN5 S327A-pLVX, $n = 14$; SEPTIN5 S327D-pLVX, $n = 13$. Morris Water Maze test: ctrl-pLVX, n = 5; SEPTIN5 WT-pLVX, n = 6; SEPTIN5 S327A-pLVX and SEPTIN5 S327D-pLVX, $n = 8$). Mean ± SEM, One-way and Two-away ANOVA, $p > 0.05$.

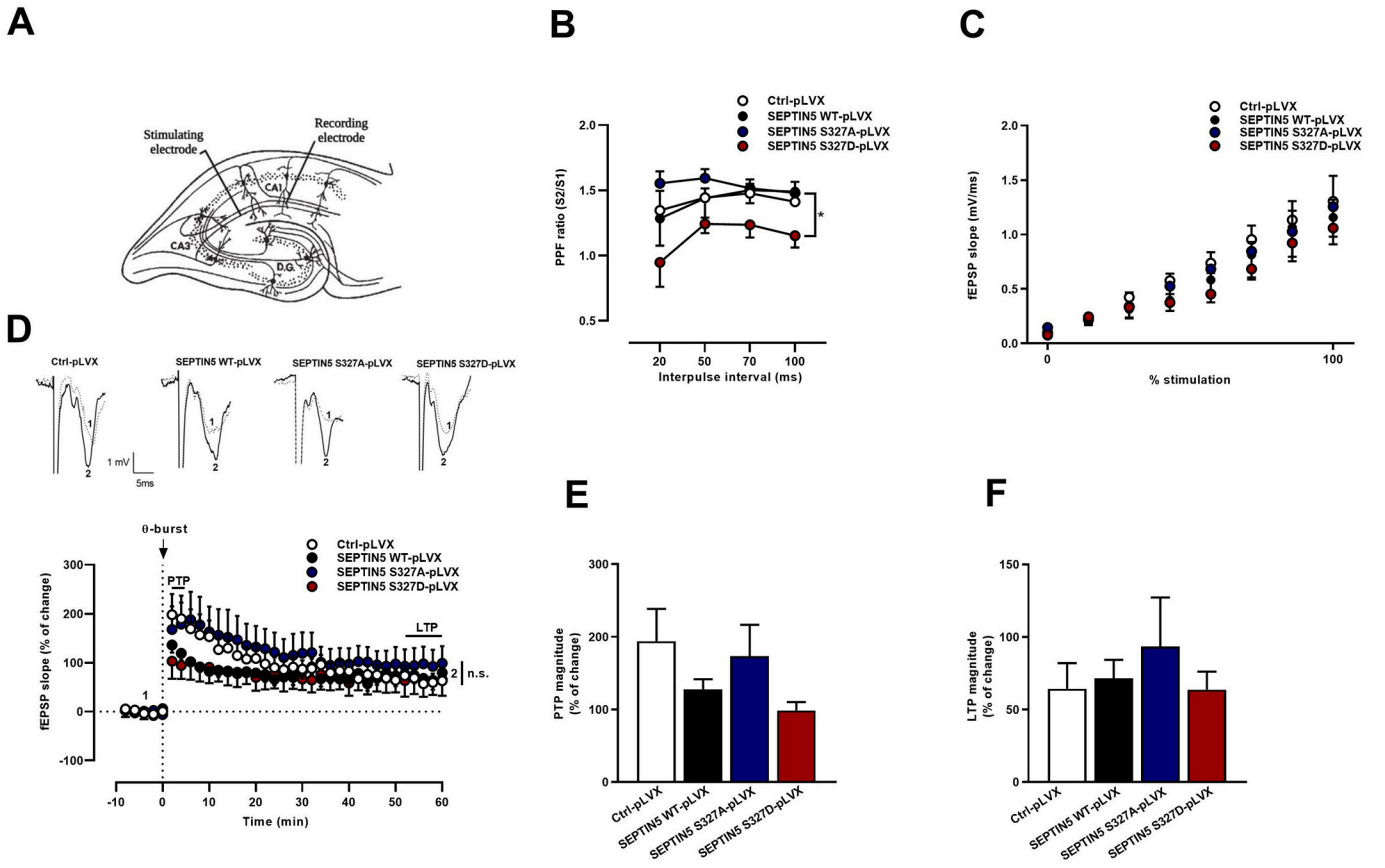


**Fig. 6.** Electrophysiological recordings to characterize the synaptic plasticity of mice intrahippocampally injected with lentiviral ctrl-pLVX, SEPTIN5 WT-pLVX, SEPTIN5 S327A-pLVX and SEPTIN5 S327D-pLVX constructs. A) Schematic representation of electrode placement in the hippocampal slice for recordings in the CA3-CA1 synapse. B) PPF across different interpulse intervals (20–100 ms). C) I/O curves represented as fEPSP *versus* percentage of stimulation to normalize the stimulation intensities required in different experiments, where 0% stimulation represents the stimulus intensity that starts to elicit a fEPSP response, and 100% stimulation represents the stimulus intensity that elicits a maximum fEPSP response. D) Representative traces prior (1) and after (2) LTP induction by theta-burst stimulation ($\theta$-burst, four trains with four pulses each at 100 Hz, separated by 200 ms), accompanied by average time course changes in fEPSP slope upon LTP induction by $\theta$-burst stimulation protocol. E) PTP magnitude after $\theta$-burst stimulation (change in fEPSP slope at 0–4 min, compared to baseline). F. LTP magnitude after $\theta$-burst stimulation (change in fEPSP slope at 50–60 min, compared to baseline). The values in the vertical axis in E and F represent the percentage of change of fEPSP slope after LTP induction as compared to baseline fEPSP for each condition. n = 5–9 (PPF: ctrl-pLVX, $n = 9$; SEPTIN5 WT-pLVX, n = 9; SEPTIN5 S327A-pLVX, n = 6; SEPTIN5 S327D-pLVX, $n = 5$. I/O curves: ctrl-pLVX, n = 9; SEPTIN5 WT-pLVX, $n = 7$; SEPTIN5 S327A-pLVX, n = 7; SEPTIN5 S327D-pLVX, $n = 4$. PTP and LTP: ctrl-pLVX, n = 9; SEPTIN5 WT-pLVX, n = 6; SEPTIN5 S327A-pLVX, n = 8; SEPTIN5 S327D-pLVX, n = 6). Mean ± SEM, One-way ANOVA, $p > 0.05$, repeated-measures ANOVA, *post hoc* Tukey HSD * $p < 0.05$.

not significant, a tendency to a decrease in PTP magnitude was apparent in slices from SEPTIN5 WT-pLVX and SEPTIN5 S327D-pLVX when compared to the ctrl-pLVX and SEPTIN5 S327A-pLVX ($p > 0.05$, one-way ANOVA, n = 6–9, Fig. 6E). This suggested a presynaptic alteration since PTP, a form of short-term synaptic plasticity, is generally thought to largely reflect presynaptic activity (Bao et al., 1997). Taken together, these data demonstrate that phosphorylation of SEPTIN5 at its functionally relevant site S327 regulates the short-term synaptic plasticity *ex vivo*.

## 4. Discussion

Several septin family members take part in biological processes aberrantly affected in AD pathogenesis, namely APP processing, autophagy, and synaptic function (Marttinen et al., 2015). Despite this evident link, studies addressing the mechanistic role of septins in AD pathogenesis remain elusive. Here, we have delineated the role of SEPTIN5 in the cellular processes relevant for AD pathogenesis. Significant transcriptional, translational and PTMs (phosphorylation in SEPTIN5) were found to correlate with the severity of neurofibrillary pathology in the human brain. Specifically, we observed a significant reduction in the RNA and protein levels of SEPTIN5 at the later stages of AD together with a significant increase in the levels of S327 phosphorylated SEPTIN5 already present in the early stages of AD-related neurofibrillary pathology in the temporal cortex. This did not correlate with the levels of SEPTIN5 and SEPTIN5 S327 phosphoepitope, or the ratio of SEPTIN5 S327/SEPTIN5 detected in the CSF samples from individuals in the early stages of AD (MCI due to AD) as compared to individuals with cognitive complaints, but who showed no biomarkers for Aβ deposition or neuronal injury (control group). This suggests that SEPTIN5 or its S327 phosphorylated form are not necessarily feasible CSF targets to be used as biomarkers for early AD. However, it remains to be established whether these targets could be useful for the monitoring of the disease progression in longitudinal study cohorts. Nevertheless, our data related to the levels of SEPTIN5 and its phosphorylated S327 form in the rat hippocampus presenting initial cognitive decline (Pinho et al., 2017) did not show differences upon aging, suggesting that alterations in the levels of S327 phosphorylation may be specifically related to the cellular processes relevant for AD rather than physiological aging.

As a significant increase in the levels of a phosphopeptide detecting the functionally relevant SEPTIN5 S327 epitope was observed in human temporal cortex within the early stages of AD-related neurofibrillary pathology, we sought to understand the consequences of SEPTIN5 S327

phosphorylation on the regulation of APP processing and the generation of Aβ as well as autophagy in the mouse cortical neurons. These processes were set as targets since the downregulation of SEPTIN5 was recently shown to lead to increased autophagosomal degradation of APP C-terminal fragments as well as Aβ clearance in the neuronal cells (Marttinen et al., 2020). Furthermore, SEPTIN5 interacts with another septin family member, SEPTIN8, which in turn has been shown to regulate the generation of Aβ *via* mechanisms altering the intracellular sorting and accumulation of BACE1 (Kurkinen et al., 2016). Importantly, most of the alterations observed in SEPTIN5 WT-overexpressing mouse primary cortical neurons, such as increased levels of BACE1 and LC3II as well as the ratio of APPm/im, were averted by excluding SEPTIN5 S327 phosphorylation. There were no significant effects on the levels of Aβ or APP CTFs upon the overexpression of SEPTIN5 WT or mutant constructs in mouse primary cortical neurons. In this context, it should be emphasized that the primary mouse cortical neuron cultures, where Septin5 was downregulated with RNA interference, showed a significantly reduced the ratio of APPm/im, which was also detected in the brain tissue of *Septin5* knock-out mice (Marttinen et al., 2020). Thus, the opposite effect was observed in the present study upon the overexpression of SEPTIN5 WT, as indicated by the significantly increased the ratio of APPm/im. This suggests that SEPTIN5 may specifically affect APP trafficking through the secretory pathway in polarized cells, such as primary neurons *via* a mechanism that is dependent on the S327 phosphorylation status of SEPTIN5. Interestingly, SEPTIN5 S327D mutant, which was designed to mimic the phosphorylated protein (phosphomimetic), was the only construct significantly reducing the levels of sAPPα and sAPPtot in the culture medium samples. It should be noted that SEPTIN5 WT and S327A also showed a similar, but a non-significant decrease in the levels of sAPPtot. In turn, the levels of BACE1 were significantly increased in the SEPTIN5 WT-overexpressing mouse cortical neurons, while this effect was averted by blocking the S327 phosphorylation of SEPTIN5. Once again, this effect was opposite to that observed in the brain tissue of *Septin5* knock-out mice, which showed a moderate reduction in the levels of BACE1 (Marttinen et al., 2020). As the recent findings have suggested a role for autophagy in the degradation of BACE1 (Feng et al., 2017; Zhang et al., 2012), it is possible that the SEPTIN5 S327-specific increase in the levels of BACE1 levels could be related to reduced autophagosomal activity in the SEPTIN5 WT overexpressing cortical neurons. Alternatively, it is possible that the overexpression of SEPTIN5 WT in its S327 phosphorylated form may influence the function of SEPTIN5 interaction partner, SEPTIN8, and consequently, reduce the turnover of BACE1 as it has been shown that SEPTIN8 modulates intracellular trafficking and degradation of BACE1 (Bläser et al., 2002; Kurkinen et al., 2016). These results together with our prior findings suggest that SEPTIN5 specifically affects APP trafficking in polarized cells through the secretory pathway in a S327-dependent manner. However, the functional relevance of the SEPTIN5 S327D phosphomimetic variant remains elusive in terms of APP processing as one would expect to see similar effects that were observed in SEPTIN5 WT-transduced cortical neurons. Instead, SEPTIN5 S327A and S327D variants showed phenotypically similar readouts in transduced cortical neurons, which were different from those observed in SEPTIN5 WT-transduced cortical neurons. In addition, SEPTIN5 S327D-transduced cortical neurons displayed a specific alteration in APP processing as a significant reduction in the culture medium levels of sAPPα was detected.

It has been previously shown that the downregulation of SEPTIN2 or SEPTIN9 leads to a robust decrease in the levels of LC3 and p62 in non-neuronal cells, suggesting that these septins are central components of the autophagosomal pathway (Mostowy et al., 2010). Similarly, the downregulation of SEPTIN5 in the human neuroblastoma cells, mouse primary cortical neurons, and in the brain tissue of *Septin5* knock-out mice resulted in decrease in the levels of LC3I and LC3II, suggesting that reducing the levels of SEPTIN5 promoted autophagosomal activity in the neuronal cells (Marttinen et al., 2020). Furthermore, a significant decrease in the levels of p62 was also observed in the neuroblastoma cells, in which SEPTIN5 was downregulated, and a similar trend was also detected in mouse cortical neurons upon downregulation of Septin5 (Marttinen et al., 2020). Thus, these previous results are in line with the findings observed in the present study, showing a significant increase in the levels of LC3II in SEPTIN5 WT-overexpressing mouse cortical neurons. These results suggest that the effects on LC3 regulation depend on the prevailing levels of SEPTIN5. Interestingly, the SEPTIN5 S327D mutant led to an increasing but a non-significant trend in LC3 levels similar to SEPTIN5 WT, while blocking the S327 phosphorylation prevented the LC3 increase. These results suggest that the S327D phosphomutant designed to mimic the phosphorylated SEPTIN5 protein is functionally active as it exerts similar effects on key autophagy-related markers to SEPTIN5 WT. However, it should be noted that because variable effects were observed with SEPTIN5 WT and S327D constructs in terms of APP processing, further studies focused on determining whether the WT or mutant SEPTIN5 differentially interact with other septins and whether they show similar or different subcellular localization to the endogenous SEPTIN5 are still needed to ascertain the functionality of S327D phosphomimetic mutant. Finally, the overexpression of SEPTIN5 WT or blocking the SEPTIN5 S327 phosphorylation did not influence neuronal viability or the production of TNF-α in the primary mouse cortical neuron-BV2 co-cultures in the basal conditions or LPS and IFNγ-induced inflammation. This suggests that neuronal survival in not dependent on the levels or S327 phosphorylation status of SEPTIN5. Also, these findings suggest that the SEPTIN5 overexpressing neurons do not secrete components, which could affect in a non-autonomous manner the inflammatory response of microglia upon the induction of inflammation.

Taking these findings in consideration together with the previous knowledge that SEPTIN5 is implicated in presynaptic release (Amin et al., 2008), we anticipated that overexpression of different SEPTIN5 phosphomutants would have an impact on synaptic function and behavior. SEPTIN5 has been associated to mechanisms of priming/docking of synaptic vesicles at the pre-fusion stage (Yang et al., 2010). Additionally, SEPTIN5 was shown to interact with syntaxin-1, a key component of the SNARE complex, in a phosphorylation dependent manner (Taniguchi et al., 2007). Constitutive phosphorylation of SEPTIN5 by CDK5 at its major phosphorylation site, the S327 residue, reduces the interaction of SEPTIN5 with syntaxin-1 impairing secretion (Amin et al., 2008), whereas the deactivation of the phosphorylation site of SEPTIN5 S327 results in a more efficient SEPTIN5-syntaxin-1 interaction thus potentiating exocytosis (Amin et al., 2008). Syntaxin-1 is required for synaptic vesicles docking and fusion (Vardar et al., 2016), and its interaction with SEPTIN5 might allow efficient vesicle priming/positioning for release. Phosphorylation of SEPTIN5 by decreasing SEPTIN5-syntaxin-1 interaction would result in reduced vesicle positioning to docking. On the contrary, overexpression of the SEPTIN5 S327A might be expected to potentiate release by increasing SEPTIN5-syntaxin-1 binding.

Mice overexpressing SEPTIN5 or its S327 phosphomutants forms did not show any cognitive or behavioral deficits. In fact, previous reports of genetic manipulation of the *Septin5* gene, revealed only mild behavioral deficits, namely decreased anxiety-related behavior (Harper et al., 2012; Suzuki et al., 2009). We had hypothesized that manipulation at a postnatal period might allow us to overcome the reported redundancy of roles within the septin family, but the relatively short time of expression period (five to six weeks) of our manipulation, leading to very localized alteration of SEPTIN5 may have precluded our ability to measure small changes in behavior. It would be interesting to evaluate if a similar strategy in an AD mouse model might accelerate disease progression.

After behavioral tests, C57BL/6 mice were used to prepare acute hippocampal slices to investigate pre- and postsynaptic changes applied by suitable PPF and LTP protocols, respectively. We found that only the lentiviral SEPTIN5 S327D construct altered PPF, decreasing the ratio across all stimulus intervals. Normally hippocampal synapses when

stimulated in short interval period display PPF. Classically, this form of short-term synaptic plasticity has been associated to the accumulation of calcium in active zones leading to larger release of neurotransmitters from presynaptic terminals upon the second stimulation (Katz et al., 1993). According to this hypothesis, a decrease in PPF is generally associated to increases in the release probability (McNaughton, 1982). However, according to the hypothesis put forward for SEPTIN5 involvement in release, it seems unlikely that calcium regulation should account for the effects observed, since calcium dependence of neurotransmitter release as measured by "calcium channel/domain cooperativity" is not different in SEPTIN5 *knockout* mice (Yang et al., 2010). Our data suggest that the overall decrease in PPF ratio should be interpreted as a decrease in the initial probability of release due to less efficient vesicle-positioning at active zones, independent of presynaptic calcium dynamics.

One could speculate that this mechanism might be more relevant in situations of high synaptic activity demand, which require vesicle recruitment beyond the readily releasable pool (RRP) which comprises few vesicles that are docked at the plasma membrane and primed for immediate fusion upon stimulation (Denker et al., 2009; Denker and Rizzoli, 2010). After the RRP has been depleted during moderate physiological stimulation, other vesicular pools can be recruited under more intense stimulation, such as paired-pulse stimulation or LTP inducing protocols (Fernandez-Alfonso and Ryan, 2008; Ikeda and Bekkers, 2009). Our data are consistent with a role of SEPTIN5 phosphorylation in the mechanisms of recruitment and positioning of vesicles from the non-RRP. The effect of SEPTIN5 phosphorylation using a protocol that relies on presynaptic mechanisms was able to evidence the role of SEPTIN5 in vesicle release dynamics, while in basal transmission or in LTP magnitude, which have marked postsynaptic mechanisms involved, no significant alterations were detected. In addition, in slices with increased levels of phosphorylated SEPTIN5 (SEPTIN5 S327D and SEPTIN5 WT), PTP tended to be lower, albeit not statistically different, than in conditions with decreased SEPTIN5 phosphorylation (SEPTIN5 S327A and control). It should be noted that the subtle alterations in PTP might also correlate with the restricted and modest expression of the SEPTIN5 forms, suggesting that a larger impact of S327 phosphorylation to synaptic function might take place in situations where this its levels are increased, such as in AD brain.

In conclusion, we report here significant alterations in SEPTIN5 expression and phosphorylation in human temporal cortex with an increasing degree of AD-related neurofibrillary pathology. Mechanistic investigations, together with the previous data regarding the effects of SEPTIN5 downregulation, suggest a role for SEPTIN5 as a regulatory component of APP trafficking and autophagy. Importantly, our findings particularly underscore the importance of phosphorylation-dependent functionality of SEPTIN5 in these processes as well as in the regulation of synaptic plasticity, all of which are substantially altered during the pathogenesis of AD. These findings coupled with the evidence that SEPTIN5 S327 site is predominantly phosphorylated by CDK5 upon AD-associated pathological stimuli warrant further studies to determine the precise role of SEPTIN5 and its S327 phosphorylation site in AD molecular pathogenesis.

## Funding

This work was supported by the Academy of Finland (grant numbers 307866, 330178 and 315459); Sigrid Jusélius Foundation; the Strategic Neuroscience Funding of the University of Eastern Finland; Fundação para a Ciência e Tecnologia (grant numbers PD/BD/128390/2017, SFRH/BD/118238/2016, PD/BD/114441/2016, PD/BD/128091/2016, PD/BD/114337/2016, and PTDC/MED-NEU/27946/2017); Santa Casa da Misericórdia de Lisboa (grant number MB-37-2017); SynaNet (LISBOA-01-0145-FEDER-0073919 under the grant agreement no. 692340).

## Declaration of Competing Interest

Authors declare no competing interests.

## Acknowledgments

We would like to thank Sara Pinto for the help provided in the electrophysiological experiments. The authors also thank to Memoclínica for the facilities provided.

## Appendix A. Supplementary data

Supplementary data to this article can be found online at https://doi.org/10.1016/j.nbd.2021.105603.

## References

Ageta-Ishihara, N., et al., 2013. Chronic overload of SEPT4, a parkin substrate that aggregates in Parkinson's disease, causes behavioral alterations but not neurodegeneration in mice. Mol. Brain. 6, 35.
Albert, M.S., et al., 2011. The diagnosis of mild cognitive impairment due to Alzheimer's disease: recommendations from the National Institute on Aging-Alzheimer's Association workgroups on diagnostic guidelines for Alzheimer's disease. Alzheimers Dement. 7, 270–279.
Amin, N.D., et al., 2008. Cyclin-dependent kinase 5 phosphorylation of human septin SEPT5 (hCDCrel-1) modulates exocytosis. J. Neurosci. 28, 3631–3643.
Anderson, W.W., Collingridge, G.L., 2007. Capabilities of the WinLTP data acquisition program extending beyond basic LTP experimental functions. J. Neurosci. Methods 162, 346–356.
Bao, J.-X., Kandel, E.R., Hawkins, R.D., 1997. Involvement of pre- and postsynaptic mechanisms in Posttetanic potentiation at Aplysia synapses. Science. 275, 969.
Batalha, V.L., et al., 2013. Adenosine a(2A) receptor blockade reverts hippocampal stress-induced deficits and restores corticosterone circadian oscillation. Mol. Psychiatry 18, 320–331.
Batalha, V.L., et al., 2016. The caffeine-binding adenosine A2A receptor induces age-like HPA-axis dysfunction by targeting glucocorticoid receptor function. Sci. Rep. 6, 31493.
Beites, C.L., Campbell, K.A., Trimble, W.S., 2005. The septin Sept5/CDCrel-1 competes with alpha-SNAP for binding to the SNARE complex. Biochem. J. 385, 347–353.
Bläser, S., et al., 2002. Human septin-septin interaction: CDCrel-1 partners with KIAA0202. FEBS Lett. 519, 169–172.
Bliss, T.V., Collingridge, G.L., 1993. A synaptic model of memory: long-term potentiation in the hippocampus. Nature. 361, 31–39.
Braak, H., et al., 2006. Staging of Alzheimer disease-associated neurofibrillary pathology using paraffin sections and immunocytochemistry. Acta Neuropathol. 112, 389–404.
Collins, M.A., et al., 2015. Total protein is an effective loading control for cerebrospinal fluid western blots. J. Neurosci. Methods 251, 72–82.
Czeredys, M., et al., 2013. Expression of genes encoding the calcium signalosome in cellular and transgenic models of Huntington's disease. Front. Mol. Neurosci. 6, 42.
Denker, A., Rizzoli, S.O., 2010. Synaptic vesicle pools: an update. Front. Synaptic Neurosci. 2, 135.
Denker, A., Kröhnert, K., Rizzoli, S.O., 2009. Revisiting synaptic vesicle pool localization in the Drosophila neuromuscular junction. J. Physiol. 587, 2919–2926.
Engelborghs, S., et al., 2017. Consensus guidelines for lumbar puncture in patients with neurological diseases. Alzheimers Dement (Amst.) 8, 111–126.
Feng, T., et al., 2017. Autophagy-mediated regulation of BACE1 protein trafficking and degradation. J. Biol. Chem. 292, 1679–1690.
Fernandez-Alfonso, T., Ryan, T.A., 2008. A heterogeneous "resting" pool of synaptic vesicles that is dynamically interchanged across boutons in mammalian CNS synapses. Brain Cell Biol. 36, 87–100.
Follenzi, A., Naldini, L., 2002. Generation of HIV-1 derived lentiviral vectors. Methods Enzymol. 346, 454–465.
Gozal, Y.M., et al., 2011. Aberrant septin 11 is associated with sporadic frontotemporal lobar degeneration. Mol. Neurodegener. 6, 82.
Gresa-Arribas, N., et al., 2012. Modelling neuroinflammation in vitro: a tool to test the potential neuroprotective effect of anti-inflammatory agents. PLoS One 7, e45227.
Hardy, J., Selkoe, D.J., 2002. The amyloid hypothesis of Alzheimer's disease: Progress and problems on the road to therapeutics. Science. 297, 353.
Harper, K.M., et al., 2012. Alterations of social interaction through genetic and environmental manipulation of the 22q11.2 gene Sept5 in the mouse brain. Hum. Mol. Genet. 21, 3489–3499.
Hughes, R.N., 2004. The value of spontaneous alternation behavior (SAB) as a test of retention in pharmacological investigations of memory. Neurosci. Biobehav. Rev. 28, 497–505.
Ikeda, K., Bekkers, J.M., 2009. Counting the number of releasable synaptic vesicles in a presynaptic terminal. Proc. Natl. Acad. Sci. 106, 2945.
Ito, H., et al., 2009. Sept8 controls the binding of vesicle-associated membrane protein 2 to synaptophysin. J. Neurochem. 108, 867–880.
Jack Jr., C.R., et al., 2018. NIA-AA research framework: toward a biological definition of Alzheimer's disease. Alzheimers Dement. 14, 535–562.

Katz, P.S., Kirk, M.D., Govind, C.K., 1993. Facilitation and depression at different branches of the same motor axon: evidence for presynaptic differences in release. J. Neurosci. 13, 3075–3089.
Kurkinen, K.M.A., et al., 2016. SEPT8 modulates β-amyloidogenic processing of APP by affecting the sorting and accumulation of BACE1. J. Cell Sci. 129, 2224–2238.
Liu, S.-L., et al., 2016. The role of Cdk5 in Alzheimer's disease. Mol. Neurobiol. 53, 4328–4342.
Marttinen, M., et al., 2015. Synaptic dysfunction and septin protein family members in neurodegenerative diseases. Mol. Neurodegener. 10, 16.
Marttinen, M., et al., 2019. A multiomic approach to characterize the temporal sequence in Alzheimer's disease-related pathology. Neurobiol. Dis. 124, 454–468.
Marttinen, M., et al., 2020. Presynaptic vesicle protein SEPTIN5 regulates the degradation of APP C-terminal fragments and the levels of Aβ. Cells 9 (11), 2482.
Mavrakis, M., et al., 2014. Septins promote F-actin ring formation by crosslinking actin filaments into curved bundles. Nat. Cell Biol. 16, 322–334.
McNaughton, B.L., 1982. Long-term synaptic enhancement and short-term potentiation in rat fascia dentata act through different mechanisms. J. Physiol. 324, 249–262.
Merluzzi, A.P., et al., 2018. Neurodegeneration, synaptic dysfunction, and gliosis are phenotypic of Alzheimer dementia. Neurology. 91, e436–e443.
Mostowy, S., et al., 2010. Entrapment of intracytosolic bacteria by septin cage-like structures. Cell Host Microbe 8, 433–444.
Müller, U.C., Deller, T., 2017. Editorial: the physiological functions of the APP gene family. Front. Mol. Neurosci. 10, 334.
Natunen, T., et al., 2016. Relationship between ubiquilin-1 and BACE1 in human Alzheimer's disease and APdE9 transgenic mouse brain and cell-based models. Neurobiol. Dis. 85, 187–205.
Pinho, J., et al., 2017. Enhanced LTP in aged rats: detrimental or compensatory? Neuropharmacology. 114, 12–19.
Prut, L., Belzung, C., 2003. The open field as a paradigm to measure the effects of drugs on anxiety-like behaviors: a review. Eur. J. Pharmacol. 463, 3–33.
Snyder, E.M., et al., 2005. Regulation of NMDA receptor trafficking by amyloid-beta. Nat. Neurosci. 8, 1051–1058.
Spellman, T., et al., 2015. Hippocampal-prefrontal input supports spatial encoding in working memory. Nature. 522, 309–314.
Suzuki, G., et al., 2009. Sept5 deficiency exerts pleiotropic influence on affective behaviors and cognitive functions in mice. Hum. Mol. Genet. 18, 1652–1660.
Tackenberg, C., et al., 2013. NMDA receptor subunit composition determines beta-amyloid-induced neurodegeneration and synaptic loss. Cell Death Dis. 4, e608.
Taniguchi, M., et al., 2007. Phosphorylation of adult type Sept5 (CDCrel-1) by cyclin-dependent kinase 5 inhibits interaction with syntaxin-1. J. Biol. Chem. 282, 7869–7876.
Teunissen, C.E., et al., 2014. Biobanking of CSF: international standardization to optimize biomarker development. Clin. Biochem. 47, 288–292.
Vardar, G., et al., 2016. Distinct functions of Syntaxin-1 in neuronal maintenance, synaptic vesicle docking, and fusion in mouse neurons. J. Neurosci. 36, 7911–7924.
Vorhees, C.V., Williams, M.T., 2006. Morris water maze: procedures for assessing spatial and related forms of learning and memory. Nat. Protoc. 1, 848–858.
Walf, A.A., Frye, C.A., 2007. The use of the elevated plus maze as an assay of anxiety-related behavior in rodents. Nat. Protoc. 2, 322–328.
Yang, Y.M., et al., 2010. Septins regulate developmental switching from microdomain to nanodomain coupling of ca(2+) influx to neurotransmitter release at a central synapse. Neuron. 67, 100–115.
Zhang, M., et al., 2012. Control of BACE1 degradation and APP processing by ubiquitin carboxyl-terminal hydrolase L1. J. Neurochem. 120, 1129–1138.